

GLOBUS: GLObal Building heights for Urban Studies

Harsh G. Kamath^{a,*}, Manmeet Singh^a, Lori A. Magruder^b, Zong-Liang Yang^a and Dev Niyogi^{a,c,d}

^aJackson School of Geosciences, University of Texas at Austin, Texas, USA.

^bDepartment of Aerospace Engineering and Engineering Mechanics, University of Texas at Austin, Texas, USA.

^cDepartment of Civil, Architectural and Environmental, University of Texas at Austin, Texas, USA.

^dOden Institute for Computational Engineering and Sciences, University of Texas at Austin, Texas, USA.

*email: kamath.harsh@utexas.edu

Abstract

Urban weather and climate studies continue to be important as extreme events cause economic loss and impact public health. Weather models seek to represent urban areas but are oversimplified due to data availability, especially building information. This paper introduces a novel Level of Detail-1 (LoD-1) building dataset derived from a Deep Neural Network (DNN) called GLObal Building heights for Urban Studies (GLOBUS). GLOBUS uses open-source datasets as predictors: Advanced Land Observation Satellite (ALOS) Digital Surface Model (DSM) normalized using Shuttle Radar Topography Mission (SRTM) Digital Elevation Model (DEM), Landsat population density, and building footprints. The building information from GLOBUS can be ingested in Numerical Weather Prediction (NWP) and urban energy-water balance models to study localized phenomena such as the Urban Heat Island (UHI) effect. GLOBUS has been trained and validated using the United States Geological Survey (USGS) 3DEP Light Detection and Ranging (LiDAR) data. We used data from 5 US cities for training and the model was validated over 6 cities. Performance metrics are computed at a spatial resolution of 300-meter. The Root Mean Squared Error (RMSE) and Mean Absolute Percentage Error (MAPE) were 5.15 meters and 28.8 %, respectively. The standard deviation and histogram of building heights over a 300-meter grid are well represented using GLOBUS.

1. Introduction

High-resolution building information is needed to study localized urban phenomena that are related to public health. Often Light Detection and Ranging (LiDAR) or satellite photogrammetric Digital Surface Models (DSM) are used for such applications. However, LiDAR surveys are not available globally and high-resolution photogrammetric DSM is noisy and requires additional processing to produce an exact DSM (Wang et al., 2021). Further, these datasets are not open-source, except for the LiDAR data over the United States and a few other locations worldwide. Therefore, a framework is needed to generate building information for urban studies using

computational models. These studies may include the Urban Heat Island (UHI) effect, urban energy usage, air quality and impact studies due to extreme events.

Models used to study urban climate such as the urban Weather Research and Forecasting (u-WRF) (Chen et al., 2011) represent the urban dynamics well but the bottleneck is the urban dataset. Users of uncoupled surface energy and water balance models such as the Urban Multi-scale Environmental Predictor (UMEP) (Lindberg et al., 2018) face a similar difficulty. Models often parameterize urbanization using the Local Climate Zones (LCZ) (Stewart and Oke, 2012). LCZs are an extended list of land cover classification, where the built-up land is further classified based on the Urban Canopy Parameters (UCP). Presently, the models are run with the default UCPs, thus providing an inaccurate representation of urbanization. As a result, there is bias in the prediction of urban canopy layer temperature and wind speed (Sun et al., 2021). Important UCPs that are to be considered are listed in table 1 and are the focus of this study.

Table 1. GLOBUS derived UCPs application in u-WRF UCMs

GLOBUS derived UCPs	Used by Urban Canopy Model (UCM)
Plan area fraction	Single-layer (Kusaka et al., 2001) and Multi-layer (Martilli et al., 2002; Salamanca and Martilli, 2010)
Area averaged building height	
Building surface to plan area ratio	
Histogram of building heights	Multi-layer
Mean building heights	Single-layer
Standard deviation of building heights	
Frontal area index	

LiDAR-derived urban canopy information is available for 44 CONUS cities from the National Urban Database and Access Portal Tool (NUDAPT) (Ching et al., 2009) and can be readily ingested in u-WRF. However, this database is based on the year 2009 and requires upgradation. Recently, efforts are made to extend the concept of NUDAPT to a global scale and World Urban Database and Access Portal Tool (WUDAPT) was created (Ching et al., 2018). WUDAPT consists of level-0 LCZ data and does not provide building information (LCZ data derived from Landsat-8 satellite is provided and default UCPs are used).

Deep learning has realized success in various fields allied to computer vision in the past decade (Reichstein et al., 2019). From identifying patterns in the Earth science data to downscaling and forecasting, deep learning has stretched the limits of present systems towards near-perfect outcomes in many applications (Rolnick et al., 2023). The problem of generating high-resolution building heights falls under the ambit of computer vision-based deep-learning models. Deep learning methods have been applied to generate urban datasets previously. For instance, two-dimensional building footprints have been derived from space- and air-borne imagery using semantic segmentation methods (Bittner et al., 2018) and de-noising photogrammetric DSM (Wang et al., 2021). Modeling urban DSM has been attempted using space and air-borne RGB satellite imagery employing Convolutional Neural Network (CNN) based architecture (Karatsiolis et al., 2021). Prediction of grid aggregated building heights using Sentinel-1 satellite data is also

reported (Li et al., 2020). OpenStreetMap (OSM) provides building heights for some of the cities but heights for all the buildings are not available. Therefore, Bernard et al. (2022) used Random Forest (RF) to fill the missing building heights from OSM for French cities.

In this study, we present preliminary validation results from GLOBUS. The method discussed in this paper has the potential to generate near-global building canopy information at 1-m spatial resolution. The UCPs from table 1 can be directly derived at the model's native resolution from GLOBUS 1-m output and can be ingested in the u-WRF preprocessing system (WPS).

2. Data acquisition

This section discusses the datasets used for model training and validation. For validation, areas in the city that represent high-, low-, and mid-rise buildings and their mix are selected. Figure 1 shows the cities used for training and validation overlaid on the 2013 nightlight map.

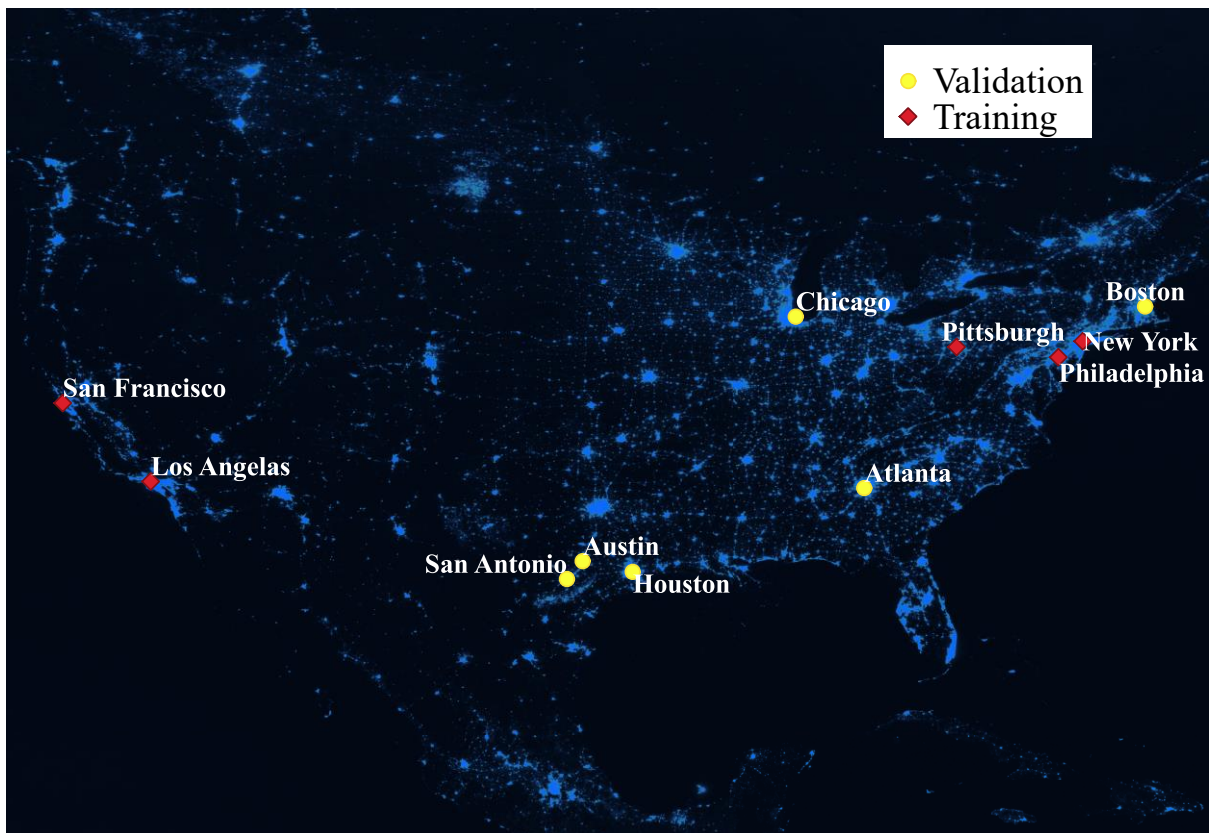


Figure 1. GLOBUS training and validation cities are marked on the 2013 nightlights map over North America.

2.1. LiDAR

United States Geological Survey (USGS) 3DEP point cloud data were used in this study. Feature class point labeling for semantic segmentation was done followed by rasterization of the building canopy layer at 1-m spatial resolution. The 1-m resolution was chosen based on the LiDAR point cloud density per square meter. Point cloud elevation averaging technique was used over 1×1 m

grid box for rasterization. Bare earth or Digital Elevation Model (DEM) was also generated from the LiDAR point cloud. LiDAR normalized building DSM (nDSM) was obtained by subtracting the building DSM from DEM. The LiDAR building nDSM was used as the target for the Deep Neural Network (DNN) training and also for validation. For a particular city, data were processed in multiple tiles of area 5 square kilometers and these tiles do not overlap.

2.2. ALOS World 3D and population density

JAXA ALOS/PRISM near-global DSM (Tadono et al., 2015) was subtracted from the Shuttle Radar Topography Mission (SRTM) DEM to obtain the space-borne nDSM at 30-m spatial resolution. This nDSM was interpolated to match the resolution of LiDAR data using cubic interpolation. This operation is needed to make the input and output images to the DNN theoretically equal in size and ensure that the training occurs as a consistent image to image regression. An elaborate explanation on the use of cubic interpolation in a similar setting can be found in Dong et al. (2015). Population density can be used as a proxy for building height as a large population confined within a small building footprint would imply taller buildings. Here, we have used globally available landscan population density data at 1-km resolution which was interpolated using a procedure similar to ALOS interpolation.

2.3. Building footprints

The present version of GLOBUS uses OSM and Microsoft global footprint vectors. The building footprint vector layer was rasterized at 1-m resolution and processed in binary format (0 = no buildings and 1 = buildings).

3. Methodology

In this section, data processing, the method used to develop the GLOBUS model and error metrics used for evaluation are discussed.

3.1. Data processing

A larger tile over a city was broken down into sub-tiles with a resolution of 256×256-m and the projection in World Geodetic System-84 (WGS 84) was preserved. After training, the predictions from the model were stitched back to reconstruct the larger tile of its original size. Min-max normalization was used to scale the predictors and the target data. All the data was processed in NETCDF4 file format and TensorFlow-2 was used for the implementation of DNN.

3.2. GLOBUS

GLOBUS DNN is based on the U-Net architecture (Ronneberger et al., 2015) and the network is graphically represented in Figure 2. It can be seen from the schematic that (i) the input and output size of the datasets corresponding to 256×256; (ii) width of the elements represented by horizontal edges reflect the number of filters used in the respective layers and (iii) slant edges are the size of images in the different layers. Hyperparameter tuning was used, and the best results were obtained for a batch size of 1 and rectified linear unit or ReLU [$\max(0,z)$] activation for the last layer of the network. The network does not produce flat rooftops as the model inherently performs regression.

Hence, building footprint vectors were used for post-processing of output to produce Level of Detail-1 (LoD-1) building information.

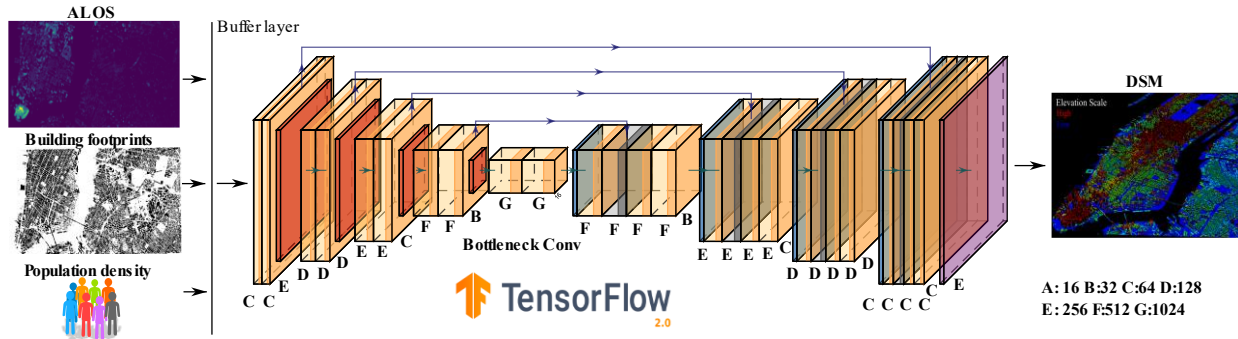


Figure 2. Schematic of UNET-based GLOBUS deep network for generation of building heights.

3.3. Validation metrics

Model parameterizations often require mean building heights and height distribution over a regular grid. The spatial resolution of this grid can range from 0.3- (local models) to 1-km (u-WRF). Similarly, 5-m vertical resolution for building heights is usually chosen for saving the storage in u-WRF. Here, we report the results over a 300-m grid. We use Root Mean Squared Error (RMSE) and Mean Absolute Percentage Error (MAPE) as error metrics for comparison against the ground truth. RMSE and MAPE are defined below

$$RMSE (m) = \sqrt{\sum_{i=1}^N (GLOBUS_i - LiDAR_i)^2 / N} \quad (1)$$

$$MAPE (\%) = \frac{100}{N} \sum_{i=1}^N |GLOBUS_i - LiDAR_i| / |LiDAR_i| \quad (2)$$

where N is the number of data points. Additionally, GLOBUS provides a histogram of building heights to represent the vertical structure of the urban fabric over a regular grid. This paper reports the building height histogram with a bin size of 5-m. The histogram at 300-m resolution was calculated by dividing the number of buildings that fall within a particular 5-m height bin derived from GLOBUS 1-m prediction by the total number of buildings within the 300-m grid.

4. Results

LiDAR building nDSM was used as ground truth for validation. The scatter plots comparing GLOBUS 300-m mean building height and standard deviation of heights with LiDAR are shown in Figure 3 along with the error metrics. Figure 3 shows that GLOBUS could predict the low- and mid-rise buildings with good accuracy and there is a large contribution of high-rise buildings towards the error. The standard deviation comparison plot shows that the distribution of building heights was captured with reasonable accuracy.

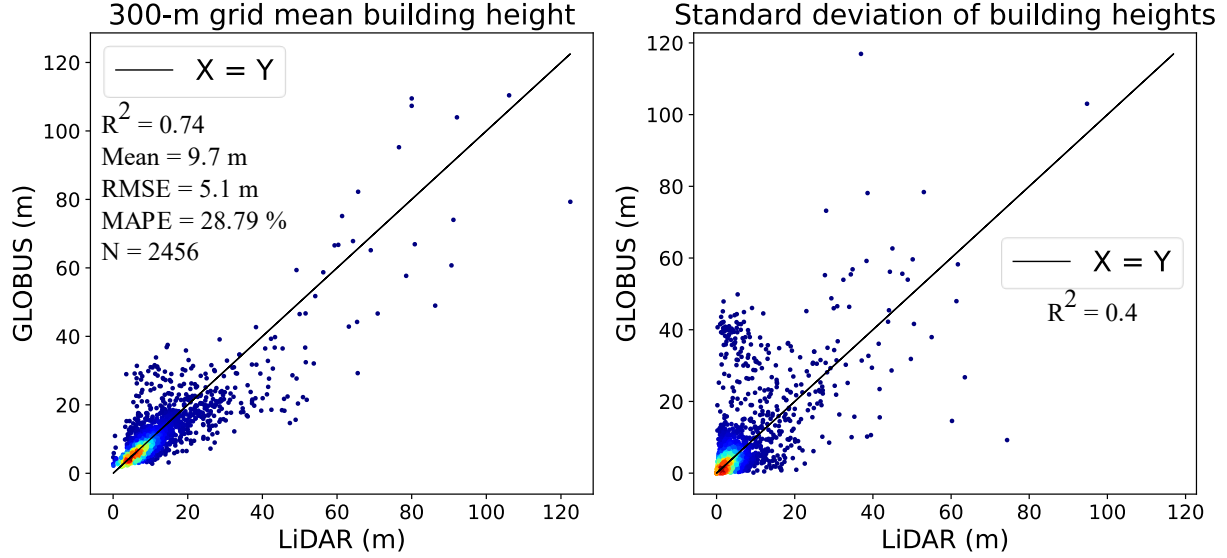


Figure 3. Scatter plots showing the validation of GLOBUS using LiDAR as the ground truth at 300-m spatial resolution.

A comparison of GLOBUS and LiDAR histograms over the downtown areas of Austin and Chicago are shown in Figure 4. We present the percentage of buildings with heights <5-m and >25-m for Austin and Chicago, respectively. The information about buildings < 5-m is crucial to estimate the canopy layer UHI using the multi-layer Urban Canopy Model (UCM) (Martilli et al., 2002). In Figure 4, the result from Figure 3 is reinforced: GLOBUS captures low and mid-rise buildings well.

Additional UCPs required by both single-layer and multi-layer UCMs are derived at 1-km spatial resolution from GLOBUS and are shown in Figure 5. The plan area fraction (λ_p) is defined as the ratio of total building footprint area to the total grid area considered.

$$\lambda_p = A_f/A_t \quad (3)$$

where A_f is the total building footprint area and A_t is total grid area. The building surface to plan area ratio (λ_b) is defined as the ratio of total building surface in the urban canopy layer (area of roofs and walls) to the grid area considered.

$$\lambda_b = (A_r + A_w)/A_t = (A_r + (P \times H))/A_t \quad (4)$$

where A_r and A_w are the roof and wall areas, respectively. Since GLOBUS generates LoD-1 buildings, λ_b can be simplified using the building footprint perimeter (P) and building height (H).

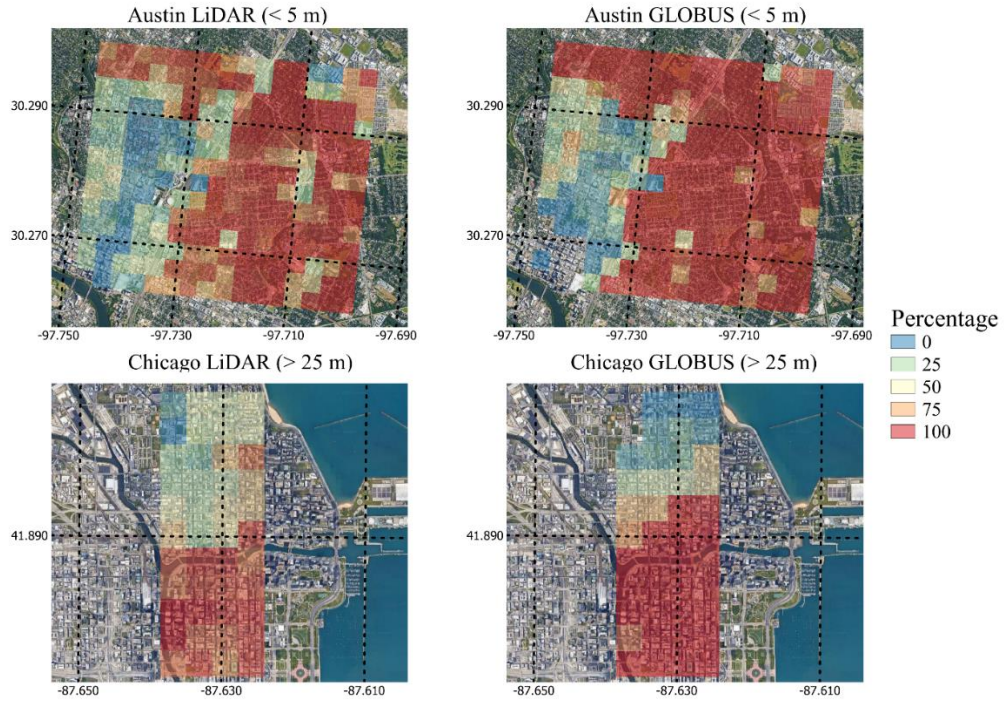


Figure 4. Histogram of building heights: percentage of buildings with heights less than 5-m in Austin downtown and buildings heights greater than 25-m in Chicago downtown. The grid resolution is 300-m.

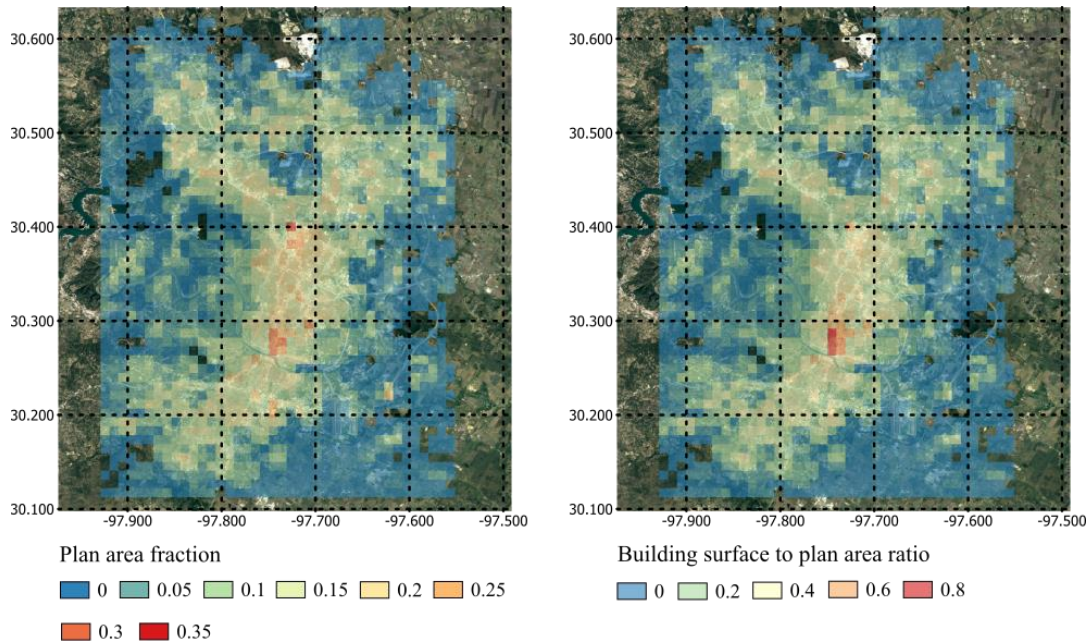


Figure 5. Plan area fraction and building surface to plan area ratio derived from GLOBUS at 1-km resolution over Austin.

5. Uncertainties

Uncertainties arise in the GLOBUS generated building heights due to the following possible reasons:

- **ALOS data:** This data was collected from 2006-11. Hence, the buildings built after this period do not appear in the data and this induces bias during training and validation. In addition, there are errors in ALOS and SRTM datasets.
- **Building footprints:** Some building footprint vectors may be missing in OSM and Microsoft global building footprint database.

6. Conclusions

We introduced the GLOBUS model that can generate near-global LoD-1 high-resolution building information. Data from GLOBUS can be readily ingested into mesoscale weather models such as u-WRF and urban-scale models such as UMEP. GLOBUS will enhance neighborhood scale urban heat mapping to design urban heat mitigation strategies and urban energy load estimations.

References

- Bernard, J., Bocher, E., Le, E., Wiederhold, S., Leconte, F., 2022. Estimation of missing building height in OpenStreetMap data : a French case study using GeoClimate 0 . 0 . 1. *Geosci. Model Dev. Discuss.* <https://doi.org/https://doi.org/10.5194/gmd-2021-428>
- Bittner, K., Adam, F., Cui, S., Körner, M., Reinartz, P., 2018. Building Footprint Extraction From VHR Remote Sensing Images Combined With Normalized DSMs Using Fused Fully Convolutional Networks. *IEEE J. Sel. Top. Appl. Earth Obs. Remote Sens.* 11, 2615–2629. <https://doi.org/10.1109/JSTARS.2018.2849363>
- Chen, F., Kusaka, H., Bornstein, R., Ching, J., Grimmond, C.S.B., Grossman-Clarke, S., Loridan, T., Manning, K.W., Martilli, A., Miao, S., Sailor, D., Salamanca, F.P., Taha, H., Tewari, M., Wang, X., Wyszogrodzki, A.A., Zhang, C., 2011. The integrated WRF/urban modelling system: Development, evaluation, and applications to urban environmental problems. *Int. J. Climatol.* 31, 273–288. <https://doi.org/10.1002/joc.2158>
- Ching, J., Brown, M., Burian, S., Chen, F., Cionco, R., Hanna, A., Hultgren, T., McPherson, T., Sailor, D., Taha And, H., Williams, D., 2009. National urban database and access portal tool. *Bull. Am. Meteorol. Soc.* 90, 1157–1168. <https://doi.org/10.1175/2009BAMS2675.1>
- Ching, J., Mills, G., Bechtel, B., See, L., Feddema, J., Wang, X., Ren, C., Brorousse, O., Martilli, A., Neophytou, M., Mouzourides, P., Stewart, I., Hanna, A., Ng, E., Foley, M., Alexander, P., Aliaga, D., Niyogi, D., Shreevastava, A., Bhalachandran, P., Masson, V., Hidalgo, J., Fung, J., Andrade, M., Baklanov, A., Dai, W., Milcinski, G., Demuzere, M., Brunsell, N., Pesaresi, M., Miao, S., Mu, Q., Chen, F., Theeuwesits, N., 2018. WUDAPT: An urban weather, climate, and environmental modeling infrastructure for the anthropocene. *Bull. Am. Meteorol. Soc.* 99, 1907–1924. <https://doi.org/10.1175/BAMS-D-16-0236.1>
- Dong, C., Loy, C.C., He, K., Tang, X., 2015. Image Super-Resolution Using Deep Convolutional Networks. *IEEE Trans. Pattern Anal. Mach. Intell.* 1–14.
- Karatsiolis, S., Kamilaris, A., Cole, I., 2021. IMG2nDSM: Height estimation from single airborne RGB images with deep learning. *Remote Sens.* 13. <https://doi.org/10.3390/rs13122417>

- Kusaka, H., Kondo, H., Kikegawa, Y., Kimura, F., 2001. A Simple Single-Layer Urban Canopy Model For Atmospheric Models: Comparison With Multi-Layer And Slab Models. *Boundary-Layer Meteorol.* 101, 329–358. <https://doi.org/10.1023/A:1019207923078>
- Li, X., Zhou, Y., Gong, P., Seto, K.C., Clinton, N., 2020. Developing a method to estimate building height from Sentinel-1 data. *Remote Sens. Environ.* 240, 111705. <https://doi.org/10.1016/j.rse.2020.111705>
- Lindberg, F., Grimmond, C.S.B., Gabey, A., Huang, B., Kent, C.W., Sun, T., Theeuwes, N.E., Järvi, L., Ward, H.C., Capel-Timms, I., Chang, Y., Jonsson, P., Krave, N., Liu, D., Meyer, D., Olofson, K.F.G., Tan, J., Wästberg, D., Xue, L., Zhang, Z., 2018. Urban Multi-scale Environmental Predictor (UMEP): An integrated tool for city-based climate services. *Environ. Model. Softw.* 99, 70–87. <https://doi.org/10.1016/j.envsoft.2017.09.020>
- Martilli, A., Clappier, A., Rotach, M.W., 2002. An urban surface exchange parameterisation for mesoscale models. *Boundary-Layer Meteorol.* 104, 261–304. <https://doi.org/10.1023/A:1016099921195>
- Reichstein, M., Camps-Valls, G., Stevens, B., Jung, M., Denzler, J., Carvalhais, N., Prabhat, 2019. Deep learning and process understanding for data-driven Earth system science. *Nature* 566, 195–204. <https://doi.org/10.1038/s41586-019-0912-1>
- Rolnick, D., Donti, P.L., Kaack, L.H., Kochanski, K., Lacoste, A., Sankaran, K., Ross, A.S., Milojevic-Dupont, N., Jaques, N., Waldman-Brown, A., Luccioni, A.S., Maharaj, T., Sherwin, E.D., Mukkavilli, S.K., Kording, K.P., Gomes, C.P., Ng, A.Y., Hassabis, D., Platt, J.C., Creutzig, F., Chayes, J., Bengio, Y., 2023. Tackling Climate Change with Machine Learning. *ACM Comput. Surv.* 55, 1–96. <https://doi.org/10.1145/3485128>
- Ronneberger, O., Fischer, P., Brox, T., 2015. U-Net: Convolutional Networks for Biomedical Image Segmentation, in: Navab, N., Hornegger, J., Wells, W.M., Frangi, A.F. (Eds.), *Lecture Notes in Computer Science (Including Subseries Lecture Notes in Artificial Intelligence and Lecture Notes in Bioinformatics)*, Lecture Notes in Computer Science. Springer International Publishing, Cham, pp. 234–241. https://doi.org/10.1007/978-3-319-24574-4_28
- Salamanca, F., Martilli, A., 2010. A new Building Energy Model coupled with an Urban Canopy Parameterization for urban climate simulations-part II. Validation with one dimension off-line simulations. *Theor. Appl. Climatol.* 99, 345–356. <https://doi.org/10.1007/s00704-009-0143-8>
- Stewart, I.D., Oke, T.R., 2012. Local climate zones for urban temperature studies. *Bull. Am. Meteorol. Soc.* 93, 1879–1900. <https://doi.org/10.1175/BAMS-D-11-00019.1>
- Sun, Y., Zhang, N., Miao, S., Kong, F., Zhang, Y., Li, N., 2021. Urban Morphological Parameters of the Main Cities in China and Their Application in the WRF Model. *J. Adv. Model. Earth Syst.* 13, 1–20. <https://doi.org/10.1029/2020MS002382>
- Tadono, T., Takaku, J., Tsutsui, K., Oda, F., Nagai, H., 2015. Status of ALOS World 3D (AW3D) global DSM generation, in: 2015 IEEE International Geoscience and Remote Sensing Symposium (IGARSS). IEEE, pp. 3822–3825. <https://doi.org/10.1109/IGARSS.2015.7326657>

Wang, Y., Zorzi, S., Bittner, K., 2021. Machine-learned 3D building vectorization from satellite imagery. *IEEE Comput. Soc. Conf. Comput. Vis. Pattern Recognit. Work.* 1072–1081.
<https://doi.org/10.1109/CVPRW53098.2021.00118>